Available online at www.sciencedirect.com

ScienceDirect

journal homepage: www.elsevier.com/locate/he

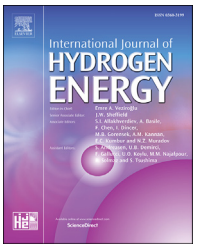

Effect of nickel on hydrogen permeation in ferritic/pearlitic low alloy steels

Hans Husby [a,*], *Mariano Iannuzzi* [a,b,1], *Roy Johnsen* [a], *Mariano Kappes* [c], *Afrooz Barnoush* [a]

[a] *Department of Engineering Design and Materials, Norwegian University of Science and Technology (NTNU), 7491 Trondheim, Norway*

[b] *GE Oil & Gas and NTNU, 1338 Sandvika, Norway*

[c] *Instituto Sabato, San Martín, Argentina*

ARTICLE INFO

Article history:
Received 8 October 2017
Received in revised form
25 December 2017
Accepted 26 December 2017

Keywords:
Oil & gas
Low alloy steel
Nickel
Hydrogen
Permeation
Embrittlement

ABSTRACT

Nickel offers several beneficial effects as an alloying element to low alloy steels. However, it is, in the oil and gas industry, limited by part 2 of the ISO 15156 standard to a maximum of 1 wt% due to sulfide stress cracking resistance concerns.

Hydrogen uptake, diffusion, and trapping were investigated in research-grade ferritic/pearlitic low alloy steels with Ni contents of 0, 1, 2 and 3 wt% by the electrochemical permeation method as a function of temperature and hydrogen charging conditions.

Qualitatively, the effective diffusion coefficient, D_{eff}, decreased with increasing Ni content. The sub-surface lattice hydrogen concentration, C_0, decreased with increasing Ni content in all charging conditions while the trend between the sub-surface hydrogen concentration in lattice and reversible trap sites, C_{OR}, and Ni content varied with the charging conditions. Irreversible trapping, evaluated by consecutive charging transients, was not observed for any of the materials. Lastly, the possible influence of an increasing fraction of pearlite with increasing Ni content is discussed.

Introduction

Low alloy steels (LAS) are widely used in the oil and gas industry due to their excellent combination of mechanical and technological properties and cost [1]. Part 2 of the ISO 15156 standard [2] regulates the use of carbon steel (CS) and LAS in H_2S-containing environments. The standard restricts the allowable nickel (Ni) content to maximum 1 wt%, due to controversial concerns regarding sulfide stress cracking (SSC) resistance [1,3]. Despite extensive investigations from the mid-1960s to late 1980s, the engineering community has yet to reach consensus as to whether the cap on Ni is scientifically justified. ISO 15156 allows the use of steels that exceed the strength, hardness, and composition requirements if successfully qualified as per the procedures described in Annex B of the specification. In practice, however, the 1 wt% Ni limit excludes LAS families with superior mechanical and technological properties that contain above 2–3 wt% Ni, such as ASTM (American Society for Testing and Materials, West Conshohocken, PA) A508 Grade 4, 10GN2MF2 and UNS K32047, from sour service applications [4]. In this regard, Ni improves LAS hardenability, fatigue life and toughness, and lowers the ductile to brittle transition temperature with a moderate penalty on weldability [1]. Qualifying LAS with Ni contents

* *Corresponding author.*
E-mail address: hans.husby@ntnu.no (H. Husby).
[1] Currently at Curtin University, Perth, Australia.

https://doi.org/10.1016/j.ijhydene.2017.12.174
0360-3199/

above 1 wt% could benefit the development of sour reservoirs with severe temperature and pressure conditions [1]. A comprehensive overview of the effects of nickel on LAS performance can be consulted elsewhere [1].

Hydrogen embrittlement (HE) is a generic term referring to the embrittlement of a material caused by the presence of atomic or nascent hydrogen [5]. HE groups various environmentally assisted cracking mechanisms such as hydrogen stress cracking (HSC) and SSC [5]. HSC results from the combination of tensile stress and atomic hydrogen in the metal [6]. Hydrogen uptake, diffusion, and trapping have been shown to affect cracking resistance [7–11]. In this regard, SSC is considered a form of HSC in the presence of H_2S [12]. Ni affects these properties, both directly as an element in solid solution, and indirectly due to its refining effect [13] on the microstructure. As part of a broader effort to quantify Ni's role on the overall HE susceptibility of LAS, this work focuses on the effect of Ni in solid solution in the body center cubic (bcc) ferrite phase on hydrogen permeation.

LAS are primarily used in the quenched and tempered (QT) condition. The effect of Ni on hydrogen permeation in such steels has been investigated previously by, e.g., Wilde et al. [14] and Yoshino and Minozaki [15]. In both cases, the effective diffusion coefficient, D_{eff}, decreased with increasing Ni content. D_{eff} is the apparent diffusion coefficient found from fitting a hydrogen permeation transient to Fick's second law as described in section Analysis of the results. However, no conclusions can be drawn about the effect of Ni present in solid solution in the ferrite phase from the results on QT steels.

Beck et al. [16] investigated hydrogen permeation in pure Fe-Ni alloys at temperatures from 27 to 90 °C. The authors assumed purely ferritic microstructures up to 8 wt% Ni, which was later questioned by others [17,18]. D_{eff} decreased and the hydrogen content increased with increasing Ni content. Dresler and Frohberg [17] performed permeation experiments at 25 °C on Fe-Ni alloys, which, according to the authors, had ferritic microstructures up to 5 at% (~5 wt%) Ni. D_{eff} decreased slightly with increasing Ni content. However, hydrogen concentrations were not estimated. Likewise, consecutive permeation transients to evaluate whether trapping was reversible or irreversible were not performed in either of the investigations. Moreover, all CS and LAS contain interstitial carbon, which may influence hydrogen permeation alone [19] and in combination with Ni in solid solution.

Quantifying the effects of Ni as a solid solution element in the ferrite phase on hydrogen uptake, diffusion, and trapping is essential to gain a fundamental understanding of the HE performance of nickel-containing LAS. This work describes the electrochemical hydrogen permeation testing of ferritic/pearlitic research-grade LAS whose chemistries differed only by their Ni contents.

Experimental

Materials

Research-grade LAS plates that varied only in their Ni content were fabricated for the project. The nominal Ni concentrations were 0, 1, 2 and 3 wt%. The actual chemical compositions are shown in Table 1. The alloys were vacuum induction melted in an alumina crucible at 1600 °C. They were fully "killed" (i.e., deoxidized) and fine grain treated by aluminum addition. Calcium was added for inclusion shape control.

Impurity levels were analyzed by glow discharge mass spectroscopy. Calculated *X*- (Bruscato) and *J*- (Watanabe) factors [20], presented in Table 1, reflect the ultra-low level of impurity elements present in the samples. As suggested by Kohno et al. [21], the materials can be considered immune to temper embrittlement for the purpose of this work.

Heat treatment

Materials were delivered as plates with a thickness of approximately 1 cm after casting and hot-rolling. The rolling operation resulted in plates with banded microstructures in the as-received condition. All samples were subsequently homogenized by prolonged stepwise heat treatments to eliminate the observed banding. Samples were first heated to 1200 °C for 7 days. Furnace cooling to 500 °C (i.e., below the lower transformation temperature, A_{c_1}) and reheating to 930 °C (i.e, above the upper transformation temperature, A_{c_3}) twice to refine the microstructures, followed the homogenization step. Coupons were encapsulated in quartz glass, providing a vacuum atmosphere to minimize oxidation and decarburization of the samples during homogenization. Because Ni has a strong grain refinement effect [13], a third re-austenitization step, followed by controlled cooling down to 600 °C, at a rate slower than that obtained by furnace cooling, was applied to the 2 and 3 wt% Ni samples to obtain comparable microstructures for all Ni contents. The full heat-treatment process is shown in Fig. 1.

Characterization of microstructures

The degree of banding in the as-received materials was documented in a 2 wt% Ni spare sample. The as-received material was heated to 930 °C followed by furnace cooling to 500 °C, before cooling with the furnace door open to air until reaching room temperature. Micrographs were taken normal to the rolling direction by scanning electron microscopy (SEM) using secondary electron imaging. The removal of banding by the homogenization treatment was confirmed by microstructure investigations in the SEM normal to the rolling direction in samples of all Ni contents. Likewise, the microstructures of the tested samples, one of each Ni content, were documented in the SEM after permeation testing.

Table 1 – Chemical compositions of research-grade LAS. Analyzed by manufacturer with methods specified in ASTM E1019-11/CO [22] and ASTM E1479-99/CTP3101/ICP [23].

Alloy	Ni [wt%]	Mn [wt%]	Si [wt%]	C [wt%]	*X*-factor	*J*-factor
0 wt% Ni	0.00	1.30	0.24	0.17	0.47	6.99
1 wt% Ni	0.97	1.30	0.24	0.17	0.48	7.05
2 wt% Ni	1.85	1.28	0.23	0.17	0.43	6.56
3 wt% Ni	2.86	1.30	0.24	0.17	0.59	9.09

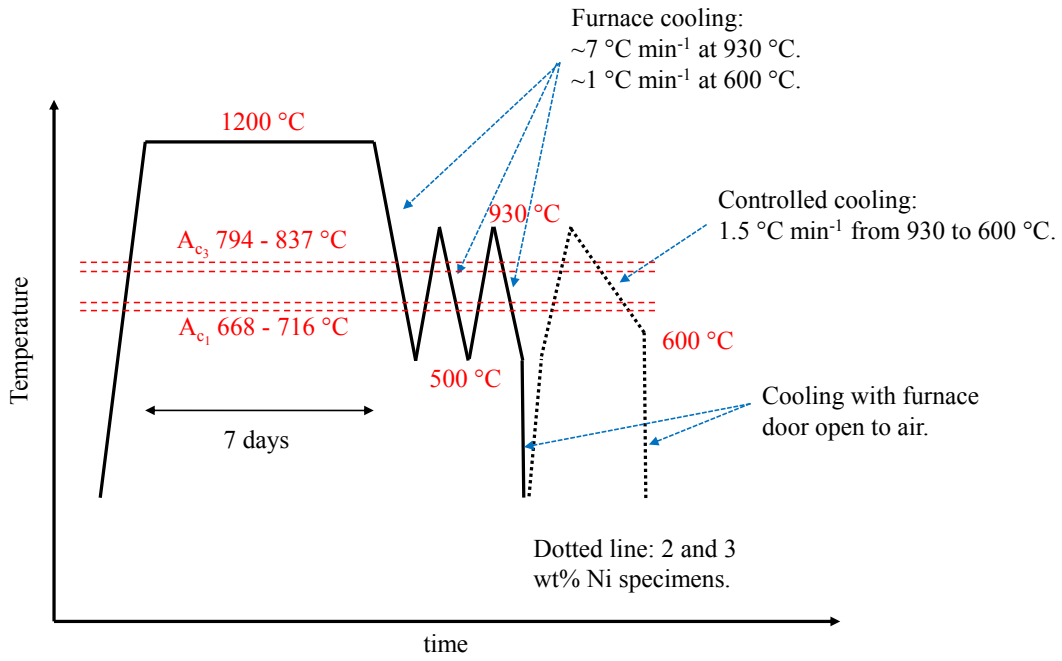

Fig. 1 – Heat treatment temperature-time procedure. All samples were heat treated according to the solid temperature-time line. Samples with 2 and 3 wt% Ni were also heat-treated as to the dashed line. Lower, A_{C_1}, and upper, A_{C_3}, austenite transformation temperatures upon heating estimated by equations from Andrews [24] for 0 and 3 wt% Ni materials are included in the figure. The lowest values of both A_{C_1} and A_{C_3}, 794 and 668 °C, respectively, are for the 3 wt% Ni material.

The characterization of grain size, interlamellar pearlite spacing, and pearlite fraction was done on a different set of samples, one of each Ni content, that was heat treated identically to the permeation samples, Fig. 1. These samples were from the same material batch as the samples for permeation experiments but prepared as rectangular rods of 1 by 1.2 by 10.2 cm.

The grain sizes were evaluated by the Heyn lineal intercept procedure and the planimetric method, both described in ASTM E112 [25]. For the line-intercept procedures, between 190 and 270 intercepts were calculated for each Ni content. In the planimetric approach, one rectangular field of microstructure was evaluated for each Ni content with an area of 0.11 mm^2. Pearlite colonies were counted as grains. The number of grains in the areas ranged from 300 to 550. The ASTM grain size no. of the materials was found by the average of the two methods.

The fractions of pearlite in the materials were evaluated by the area fractions in single fields of 0.11 mm^2. For non-oriented microstructures, the average area fraction of a phase from plane sections in the structure equals the volume fraction of that phase [26].

The pearlite interlamellar spacing was estimated as recommended by Underwood [26], through determining the mean random spacing to estimate the mean true spacing. Unbiased field selection was performed to 15 pearlite colonies in each material, a number from which Voort et al. [27] obtained adequate accuracy. Circular test grids with diameters of 2.55 μm were used to measure the mean random spacing values. The mean true spacing was, then, approximated by the half value of mean random spacing [26,27].

All microstructures were revealed by electropolishing. Before electropolishing, the samples were ground to US grit 600 (European P1200) and polished with diamond suspensions of 3 and 1 μm particle sizes. Electropolishing was performed in a commercially available electropolishing machine at 40 V for 30 s. The electrolyte was a commercial product based on perchloric acid, ethanol, and 2-Butoxyethanol designed for steels.

Hydrogen permeation experiments

Sample preparation

Samples for the permeation experiments were made using wire electrical discharge machining (EDM). All samples had diameters of 29 mm, with an exposed area of 4.91 cm^2. Sample thickness varied and is described in section Electrochemical hydrogen permeation experiments. Sample thicknesses were measured at five evenly distributed locations around the circumference to give average values. The cathodic side of the samples was ground to US grit 600 (European P1200) as recommended in ASTM G148-97 [28] and rinsed in ethanol.

The need for using a Pd coating on the anodic side of the samples to ensure efficient oxidation of hydrogen in permeation experiments has been demonstrated previously by Manolatos et al. [29] and was, therefore, applied in this work. The Pd solution was made following the process proposed by Bruzzoni [30]. In short, an aqueous solution of Na_2 $[Pd(NO_2)_4]$ was prepared by dissolving 0.18 g $PdCl_2$ in five drops of HCl (37%), approximately 0.25 ml. The solution was, then, brought to a boil, before adding 0.40 g $NaNO_2$ and 150 ml distilled water and boil for another 10 min. Subsequently, 0.20 g NaCl were

added and the solution taken off the heating plate. Finally, distilled water was added to give a total volume of 200 ml.

Before Pd deposition, samples were ground with SiC paper to U.S. grit 600 (European P1200), sonicated in ethanol and dried. Pickling was performed in volumetric 50/50 mix of 37% HCl and deionized (DI) water for the 20 s before rinsing in DI water and drying with hot air immediately before the Pd coating process. Pd electrodeposition was performed in the same cells (Fig. 2) as the hydrogen permeation experiments, using only one compartment. The deposition procedure was adapted from the methodologies first proposed by Bruzzoni et al. [31] and later Castaño Rivera et al. [32]. The deposition compartment was filled with 0.1 M NaOH and cathodic polarization was initiated at -100 μA cm^{-2}. Nitrogen gas was purged through the deposition compartment at a flow rate of 25 ml min^{-1}. After 5 min, 7 ml of the Na_2 [$Pd(NO_2)_4$] solution was added to the cell to give a concentration of 0.35 mM. The nitrogen flow was reduced to 12 ml min^{-1} 30 s after adding the Pd-solution. The cathodic current density was fixed at -100 μA cm^{-2} during the total Pd-deposition time of 60 min.

Energy dispersive spectroscopy (EDS) was used to verify the presence of Pd in one of the coated samples. A low acceleration voltage of 5 kV was used to restrict the analysis to the coating and reduce the impact of the underlying substrate. Two dummy samples of 0 wt% Ni and two dummy samples of 3 wt% Ni were weighted before and after the deposition process using a scale with a precision of 0.1 mg to provide estimates of the Pd coating thickness. Cross-sectional images of the coating were captured in the SEM. To obtain a cross-section of the coating, a 50 μm thick pure iron sheet (without grinding) was coated in the same way as the permeation samples and subsequently torn into small pieces.

Since the Pd-deposition process introduced hydrogen to the steel membranes, they were degassed overnight before the permeation experiments. Degassing was performed following Castaño Rivera et al. [32] at 120 °C for 16 h, which was 10 °C above the temperature used by the authors. According to a local equilibrium model [33], i.e., hydrogen in traps in equilibrium with hydrogen at interstitial lattice sites, the degassing process should remove hydrogen from traps with energies up to 60–70 kJ mol^{-1}. Castaño Rivera et al. [32] claimed to detect traps with energies up to 75 kJ mol^{-1} after degassing at 110 °C. In this regard, traps with energies above 60 kJ mol^{-1} are usually considered irreversible [34]. Since the time scale of the permeation discharge transients in this work was of hours, traps with energies somewhere in the range of 50–60 kJ mol^{-1} and above should be detected as irreversible, due to slow H leakage from these traps at ambient temperatures, as discussed by Turnbull [35].

Electrochemical hydrogen permeation experiments

Electrochemical hydrogen permeation experiments, as first described by Devanathan and Stachurski [36], were conducted in the custom-made glass cell assembly shown in Fig. 2. The experiments were performed in accordance with the ISO 17081 [37] and ASTM G148 [28] recommendations. The sample was clamped between two individual semi-cells and was sealed by rubber O-rings. The white polymer ring seen in Fig. 2 ensured reproducible mounting of the samples for all experiments and included the pin for the electrical connection to the sample. Each compartment had a volume of about 100 cm^3, hence satisfying the ASTM G148 recommendation of a solution-volume-to-surface-area-ratio greater than 20 ml cm^{-2} [28]. The electrolyte temperature was controlled using water circulation through the outer walls of the glass cells. Thermocouples were installed inside the anodic and cathodic cell compartments to monitor the actual temperatures. Platinum foils with total surface areas of about 3.4 cm^2 were used as counter electrodes (CE). Luggin capillaries with reference electrodes were inserted into the ports on both compartments seen in Fig. 2. The Luggin capillaries were filled with the same electrolyte as the cell compartments in which they were located. The reference electrodes were placed above the cell compartments and kept at room temperature. The type of reference electrode used varied, depending on the composition of the electrolyte. In 0.1 M NaOH the reference

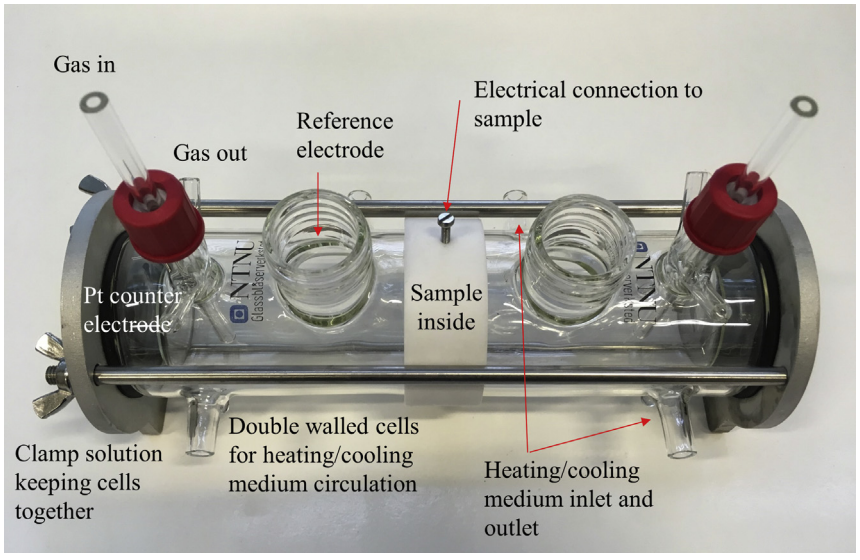

Fig. 2 – Image of custom-made glass cell assembly for electrochemical hydrogen permeation experiments.

was the mercury-mercurous electrode (MME) ($Hg/Hg_2SO_4/SO_4^{2-}$ in saturated K_2SO_4 solution) with potentials +0.41 V vs. the saturated Calomel electrode (SCE) and +0.65 V vs. the standard hydrogen electrode (SHE) at 25 °C [38]. In chloride containing electrolytes, the reference electrode was silver-silver chloride (Ag/AgCl) ($Ag/AgCl/Cl^-$ in saturated KCl solution) with potentials −0.04 V vs. SCE and +0.20 V vs. SHE at 25 °C [38].

All hydrogen permeation experiments were performed with a 0.1 M NaOH electrolyte in the anodic compartment. The anodic compartment was, in all cases, continuously purged with nitrogen gas and the sample always polarized to +300 mV_{SCE}, i.e., above the reversible hydrogen oxidation potential. The duration of hydrogen discharge before and between hydrogen charging transients varied depending on temperature and sample thickness, but were always sufficient to ensure stable background currents before charging transients. Two potentiostats with floating grounds controlled either potential or current as explained for each experiment. Experimental procedures were identical for all Ni contents under each experimental condition, (i) to (iii) described in this section.

Three types of permeation experiments were performed, and are described in i) to iii) below:

(i) *0.1 M NaOH in the cathodic compartment*: (pH = 12.2 for the aerated solution). Samples of all Ni contents were tested at 15, 45 and 70 ± 0.1 °C. For each Ni content, the same sample was used in all three temperatures, starting at 15 and ending at 70 °C. Three charge-discharge transients were performed at each temperature. At 15 °C, the consecutive transients were used to evaluate reversible and irreversible trapping as described in ISO 17081 [37]. At higher temperatures, the consecutive transients were used to test the repeatability and average the results. The initial step consisted in filling the electrolyte in both compartments and stabilize both sides at +300 mV_{SCE}. The Pd-coated anodic side stabilized at background current densities of around 0.1, 1 and 4 μA cm^{-2} at 15, 45 and 70 °C, respectively. Nitrogen was purged through the compartments both before and during the experiments to avoid oxygen contamination. The cathodic charging current density was 500 μA cm^{-2}. The cathodic side was polarized to +300 mV_{SCE} during hydrogen discharge between the transients. Sample thicknesses were about 1.9 mm. The goal of these experiments was to evaluate hydrogen uptake, diffusion, and trapping as a function of Ni content at different temperatures. Specifically, evaluating D_{eff} at three different temperatures allowed quantitative estimations of the number and strength of reversible traps in the materials as described in section Analysis of the results.

(ii) Aerated 3.5 wt% NaCl in the cathodic compartment: (pH = 5.4). Samples with 0 and 2 wt% Ni were tested at 15 ± 0.1 °C. These experiments started by stabilizing the anodic side at +300 mV_{SCE} with no electrolyte in the cathodic compartment. Nitrogen gas was purged through the cathodic compartment to minimize oxidation of the steel surface. When the background current was stable on the anodic side, the 3.5 wt% NaCl electrolyte, pre-cooled to 15 °C, was introduced into the cathodic compartment, and hydrogen charging started immediately at a potential of −1050 $mV_{Ag/AgCl}$. Nitrogen flow through the cathodic compartment was stopped at this point. Potentiostatic charging was used since the electrolyte was not deaerated. When the hydrogen permeation transient was complete, the setup was disassembled and the sample stored in a desiccator overnight. Then, the cathodic side of the sample was re-ground using SiC paper to U.S. grit 600 (P1200) and the permeation experiment repeated. Sample thicknesses were about 1.1 mm with a negligible material loss from re-grinding the cathodic sides between the transients. The objective of these experiments was to evaluate hydrogen uptake and diffusion in a different electrolyte than the conventional 0.1 M NaOH solution, tested using an identical cathodic sample surface for both transients to better evaluate reversible vs. irreversible trapping.

(iii) *Hydrogen recombination poison in the cathodic compartment*: The electrolyte in the cathodic compartment was 5 wt% NaCl + 0.5 wt% acetic acid to which thiosulfate ($S_2O_3^{2-}$) was added to a concentration of 10^{-3} M. The pH of the solution was 2.6 when aerated. The tests were performed at 15 ± 0.1 °C using 0 and 2 wt% Ni samples. Acidic thiosulfate solutions are known as alternatives to testing with H_2S gas [39,40] as H_2S gas forms locally at the steel surface [39]. A thiosulfate concentration of 10^{-3} M added to a 5% NaCl + 0.5% acetic acid solution has been found to give the highest amount of absorbed hydrogen in LAS samples at the open circuit potential (OCP) [40]. Herein, experiments started by stabilizing the anodic side at +300 mV_{SCE} without electrolyte in the cathodic compartment. Nitrogen gas was purged through the cathodic compartment to minimize oxidation of the steel surface. When the background current was stable on the anodic side, a 5 wt% NaCl electrolyte, pre-cooled to 15 °C, and free from acetic acid and thiosulfate, was introduced into the cathodic compartment. Deaeration of the cathodic compartment with nitrogen continued for 15 min. After 15 min, 96% acetic acid was injected into the cathodic compartment by syringes through a septum, followed by a thiosulfate mix (2.2 wt% $Na_2S_2O_3$ in distilled water). The NaCl solution was deaerated before adding the thiosulfate to prevent the oxidation of thiosulfate with oxygen [39]. The setup seen in Fig. 2 was modified slightly before these experiments by placing the CE inside a glass tube with a glass sinter bottom. Separating the CE via a porous membrane, allowed ion exchange while preventing oxygen production in the cell as a result of the reaction at the CE during the cathodic polarization of the sample. Acetic acid and thiosulfate should not be mixed in their concentrated forms since thiosulfate produces elemental sulfur in acids [39]. After the injection of thiosulfate, hydrogen charging was immediately commenced galvanostatically at −150 μA cm^2. Thiosulfate was used to increase hydrogen absorption during cathodic polarization as done by others [41], and not to investigate the behavior at OCP in an electrolyte simulating exposure to H_2S. The gas outlet of the cathodic cell was forced through a sodium hydroxide solution (caustic trap) to neutralize any accompanying H_2S. When the hydrogen permeation transient was complete, the setup was disassembled. The sample was stored in a desiccator overnight. Then, it was re-ground on the cathodic side and the permeation experiment repeated. Sample thicknesses were about 1.1 mm with a negligible material loss from re-grinding the

cathodic sides between the transients. The objective of these experiments was to evaluate hydrogen uptake and diffusion with higher hydrogen concentrations in the materials.

Multiple transients were conducted at each test condition, but only one set of experiments was performed per nickel content.

The test matrix was designed to investigate bulk material properties, i.e., the influence of surface processes should be minimized. The significance of surface processes as a rate-determining step increases with decreasing sample thickness [28], and diffusion experiments with samples thinner than approximately 1 mm have shown progressively decreasing diffusion coefficients with decreasing sample thicknesses [42]. Materials with faster diffusion require larger thicknesses [37], and since testing with 0.1 M NaOH in the cathodic compartment was performed up to 70 °C, it was decided to use thicker samples at the expense of the recommended 10:1 radius-to-thickness ratio in ISO 17081 [37]. The same consideration was made previously by Turnbull and Carroll [43] to ensure that the transients reflected hydrogen transport through the volume of the material and not surface controlled processes.

The reason for not selecting the extremes of Ni content when performing permeation experiments in aerated 3.5 wt% NaCl and electrolytes containing a hydrogen recombination poison was that the 2 wt% Ni samples had a microstructure closer to that of 0 wt% Ni than the 3 wt% Ni samples, as seen in section Materials characterization.

Analysis of the results

The sample sub-surface hydrogen concentration at lattice sites, C_0 in mol m^{-3}, which, as stated by Turnbull [44], is a direct reflection of the severity of the environment, was calculated using Equation (1) [37].

$$J_{ss} = \frac{I_{ss}}{F\,A} = \frac{D_l\,C_0}{L} \tag{1}$$

I_{ss} is the measured steady-state permeation current in Amperes and J_{ss} is the corresponding steady-state hydrogen flux in mol m^{-2} s^{-1}, both considered independent of trapping [9]. A is the exposed sample area in m^2 and L is the sample thickness in meters. F is Faraday's constant, 96485 C mol^{-1}. D_l is the ideal lattice diffusion coefficient in m^2 s^{-1} and can be calculated using Equation (2) [44].

$$D_l = D_0 \exp\left(\frac{-E_l}{R\,T}\right) \tag{2}$$

Where D_0 is the frequency factor in m^2 s^{-1}, E_l is the activation energy for jumps between interstitial lattice sites in J mol^{-1}, R is the gas constant in J mol^{-1} K^{-1} and T is the temperature in Kelvin [44]. D_l has been considered to be the same as for pure annealed iron, independent of metallurgical treatment and alloying, as long as the steel has a bcc structure [43]. At temperatures from −40 to 80 °C, the best representation of bcc iron is found from D_0 and E_l values of 7.23 10^{-8} m^2 s^{-1} and 5.69 kJ mol^{-1}, respectively [43].

If irreversible trapping is insignificant and the trap occupancy low (discussed in section Experimental challenges and considerations) so that the permeation transient is described by Fick's second law, the sub-surface hydrogen concentration in lattice and reversible trap sites, C_{OR} in mol m^{-3}, can be approximated by the rearrangement of Equation (3) [28,44].

$$J_{ss} = \frac{D_{eff}\,C_{0R}}{L} \tag{3}$$

D_{eff} is the effective diffusion coefficient in m^2 s^{-1}. Three methods to determine D_{eff} are described in ISO 17081 [37], and two of those have been used in this work. The t_{lag} method defines D_{eff} from the time (t_{lag} in seconds) it takes to reach J(t) $J_{ss}^{-1} = 0.63$, and is calculated from Equation (4).

$$D_{eff} = \frac{L^2}{6\,t_{lag}} \tag{4}$$

The t_b method defines D_{eff} from the time it takes for hydrogen to be detected on the anodic side after commencing hydrogen charging on the cathodic side. The breakthrough time, t_b in seconds, is determined by extrapolating the linear portion of the rising permeation transient to zero permeation flux, and D_{eff} is calculated using Equation (5).

$$D_{eff} = \frac{L^2}{15.3\,t_b} \tag{5}$$

Trap density, N_r in sites m^{-3}, and trap strength, E_b in J mol^{-1}, in a material can be estimated analytically by Equation (6) as proposed by Oriani [45]. However, there are several assumptions in this model. Namely, there must be only reversible trapping, the trap occupancy must be low and the system must be in the domain of local equilibrium [32,45,46]. Additionally, the model assumes only one type of trapping site and the traps are considered saturable, i.e., each trap can hold one H atom [32,45]. Under these conditions, D_{eff} is given by

$$D_{eff} = \frac{D_l}{1 + \frac{N_r}{N_l}\,exp\left(\frac{-E_b}{R\,T}\right)} \tag{6}$$

where N_l is the density of lattice sites in sites m^{-3}. Hydrogen atoms primarily occupy the tetrahedral interstitial sites in bcc iron at ambient temperatures (<100 °C [44]) with the corresponding N_l value of 5.2 10^{23} sites cm^{-3} [9]. Equation (6) can be re-arranged to give Equation (7). If D_{eff} is measured at several temperatures, a plot of the left hand side value of Equation (7) against the inverse of the temperature should fit to a straight line with a slope **a** and an intercept **b**, from which the values of N_r and E_b are found [32].

$$ln\left(\frac{D_l}{D_{eff}} - 1\right) = -\frac{E_b}{R\,T} + ln\left(\frac{N_r}{N_l}\right) \tag{7}$$

Results

Materials characterization

The received plate materials had severe banding along the rolling direction. Fig. 3a shows the banding microstructure in an as-received 2 wt% Ni sample heated to 930 °C followed by furnace cooling to 500 °C. The homogenization heat treatment successfully removed the banding, as confirmed by micrographs both normal and parallel to the plate rolling direction in samples of all Ni contents. Fig. 3b illustrates the removal of banding in a 2 wt% Ni sample after heat treatment as described in Fig. 1.

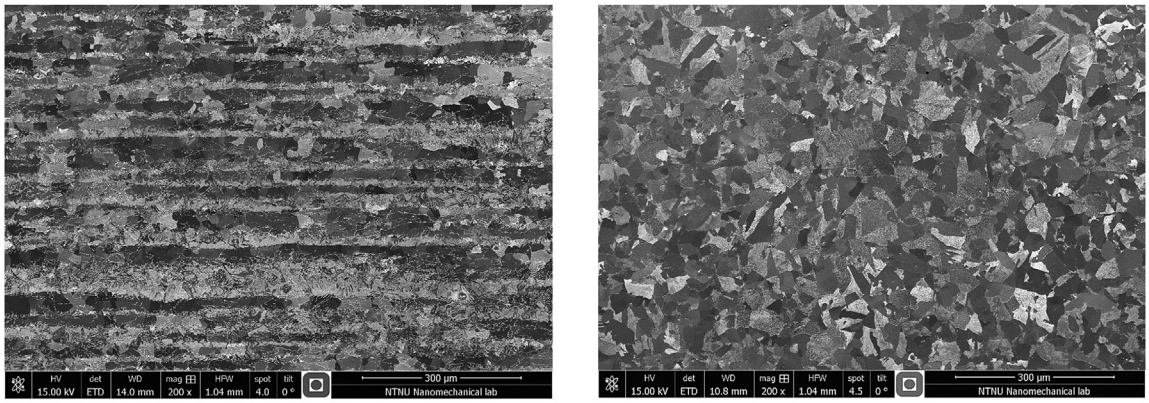

Fig. 3 – Micrograph normal to the rolling direction in a) an as-received 2 wt% Ni sample heated to 930 °C followed by furnace cooling to 500 °C and b) a 2 wt% Ni sample heat treated as described in Fig. 1.

Fig. 4 shows SEM micrographs of the permeation samples tested with 0.1 M NaOH in the cathodic compartment. All the materials had ferritic/pearlitic microstructures. The 3 wt% Ni sample had some acicular micro-constituents. In the 2 wt% Ni samples, acicular features could only be seen in a few locations.

Table 2 gives the ASTM grain size no. of the materials. The effect of Ni in refining the microstructure is seen in the difference in grain size from 0 to 1 wt% Ni, as they were heat treated following identical procedures. In contrast, samples with 2 and 3 wt% Ni were given an additional heat treatment, as described in Fig. 1. Consequently, the grain size of the 2 wt%

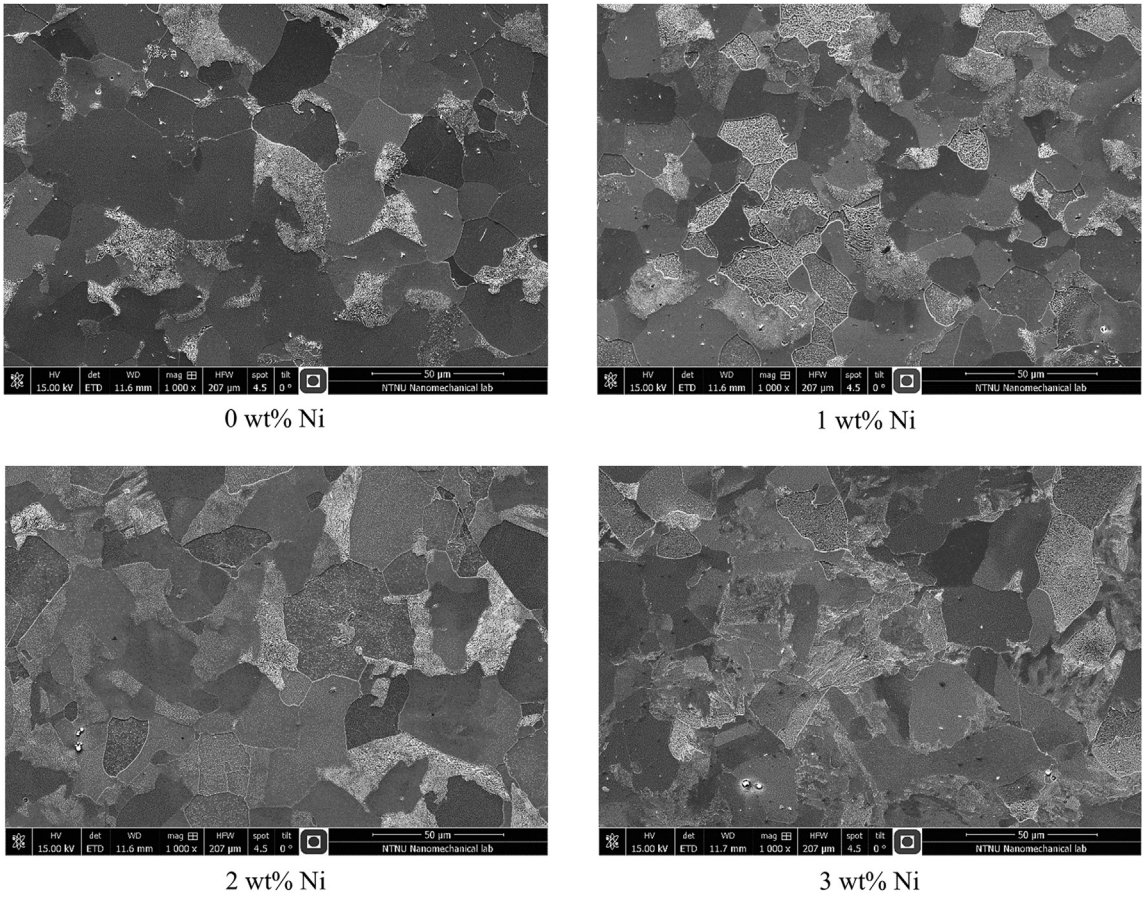

Fig. 4 – SEM micrographs of the permeation samples, 0 to 3 wt% Ni, tested with 0.1 M NaOH in the cathodic compartment, at 1000X magnification.

Table 2 – ASTM grain size no. for the LAS with different Ni contents.

Alloy	ASTM grain size no.
0 wt% Ni	8.4
1 wt% Ni	9.3
2 wt% Ni	8.8
3 wt% Ni	9.1

Ni samples fell in between the grain sizes of the 0 and 1 wt% Ni samples. The acicular and disordered microstructure in the 3 wt% Ni material reduced the reliability of quantified grain size, pearlite content and interlamellar pearlite spacing in this material.

Fig. 5 shows the pearlite fraction in the different LAS. The pearlite fraction increased from 20% to 30%, i.e., a 1.5X increase, when the Ni content changed from 0 to 3 wt%.

Fig. 6 shows the mean true interlamellar pearlite spacing of the materials. As seen in Fig. 6, the interlamellar spacing decreased in the following order: 0 wt% Ni, 2 wt% Ni, 1 wt% Ni and 3 wt% Ni.

Pd deposition

Four samples were weighted after Pd electrodeposition and the average gain was 0.25 mg (the scale had a precision of 0.1 mg). Using the density of bulk Pd of 12.0 g cm^{-3} [47], and considering the coated area, 0.25 mg corresponded to coating thicknesses of roughly 42 nm.

The Pd coating was visible to the naked eye, and EDS confirmed the presence of Pd. A surface view of a Pd-coated sample, and a cross-section of the coating obtained after tearing the 50 μm thick pure iron sheet, are shown in Fig. 7a) and b), respectively. From a cross-sectional image with higher magnification, the coating thickness was estimated to be around 200 nm. Possible reasons for the discrepancy between the theoretically estimated thickness of 42 nm and the observed 200 nm can be coating porosity, inhomogeneous Pd coverage or artifacts caused by the tearing of the iron sheet.

Hydrogen permeation experiments

0.1 M NaOH in the cathodic compartment

Fig. 8 shows the effect of Ni on the hydrogen permeation transients at 15 °C. Fig. 8 shows the second, out of three, consecutive permeation transients for each material to facilitate data visualization. Nevertheless, all permeation transients gave comparable results. The breakthrough time, t_b, increased with increasing Ni content. The permeation current density, i, decreased with increasing Ni content, except that the value for the 2 wt% Ni sample increased to roughly the same as that of the 1 wt% Ni sample after 5000 s.

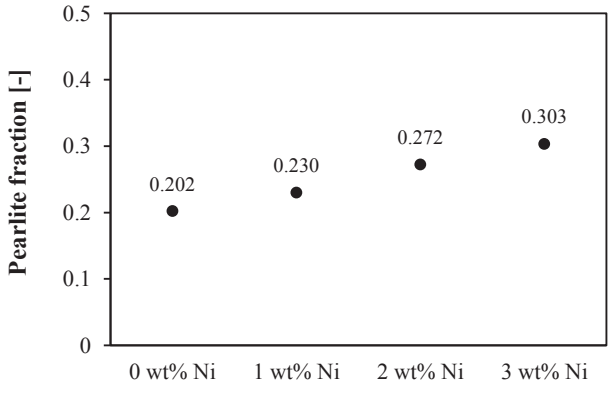

Fig. 5 – Pearlite fraction in the LAS with different Ni contents.

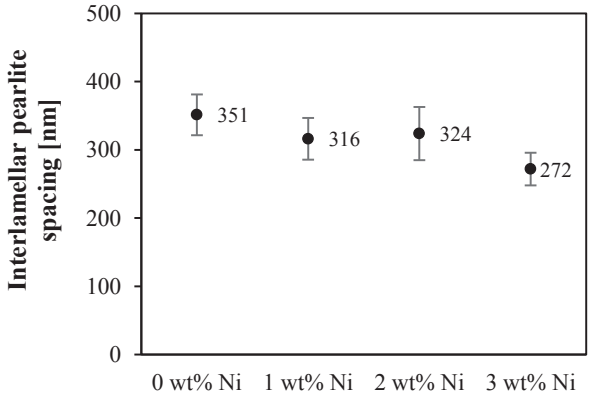

Fig. 6 – Mean true interlamellar spacing for the LAS with different Ni contents. The error bars indicate the 95% confidence intervals for the mean values.

The effect of temperature on hydrogen permeation is illustrated in Fig. 9. In Fig. 9, the second permeation transients recorded on the 3 wt% Ni samples were plotted for 15, 45 and 70 °C. t_b decreased and *i* increased with increasing temperature.

A challenge, seen in both Figs. 8 and 9, was that *i* did not stabilize at clear steady-state values. When using the t_{lag} method, the calculated D_{eff} values strongly depend on how the steady-state permeation current densities, i_{ss}, were selected. To circumvent such experimental limitations, D_{eff} values were determined by the t_b method as it is insensitive to i_{ss}. In the calculation of C_{OR} and C_0, i_{ss} values were selected 2000, 800 and 500 s after starting hydrogen charging on the cathodic side at 15, 45 and 70 °C, respectively. These times were the same for all materials when charging in 0.1 M NaOH.

With i_{ss} determined as described above and D_{eff} determined by the t_b method, C_{OR} and C_0 were obtained from all transients at all tested temperatures according to Equations (1) and (3). Fig. 10 shows D_{eff} as a function of Ni content and temperature. D_{eff} decreased with increasing Ni content at all temperatures, and the variations between the consecutive transients (seen by the error bars, which are hidden by the markers in most cases) were smaller than the variations between Ni contents.

Fig. 11 shows C_{OR} as a function of Ni content and temperature. As seen in Fig. 11, C_{OR} was independent of Ni content when charging hydrogen galvanostatically in 0.1 M NaOH. Average C_{OR} values between all Ni contents increased from 0.014 to 0.018–0.036 ppm (wt) when the temperature increased from 15 to 45–70 °C under the same charging current density.

Fig. 12 shows the thickness-normalized steady-state hydrogen permeation fluxes, J_{ss} L, as a function of Ni content and temperature. J_{ss} L decreased with increasing Ni content at all temperatures, except for 1 and 2 wt% Ni samples at 45 °C. J_{ss} L increased with increasing temperature for all Ni contents.

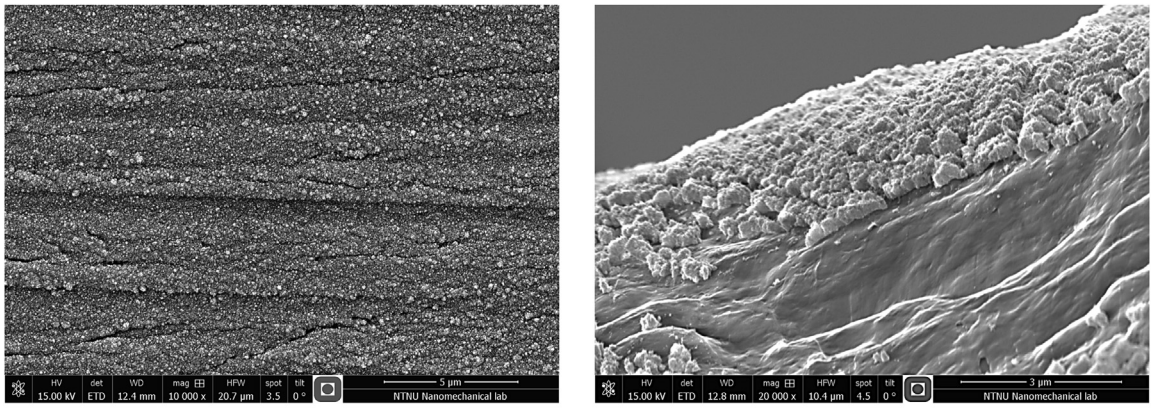

Fig. 7 – SEM images of the Pd coating used on the anodic side of the samples, a) seen top down on a permeation sample and b) seen cross-sectional after tearing a coated 50 μm thick pure iron sheet.

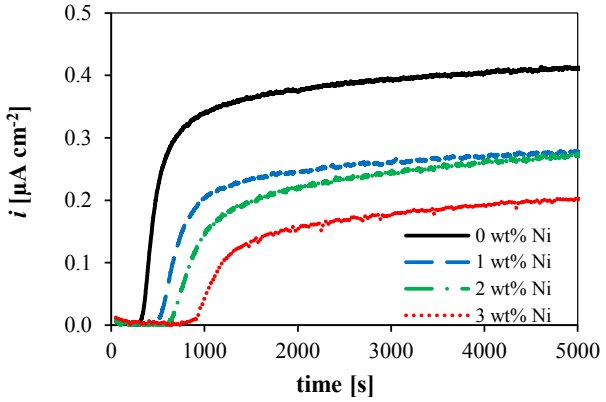

Fig. 8 – Second permeation transients (out of three consecutive), for all Ni contents, when charging in 0.1 M NaOH at 15 °C. The largest difference in sample thickness between two samples was 0.02 mm [1% of total sample thickness], hence normalized axes are not used.

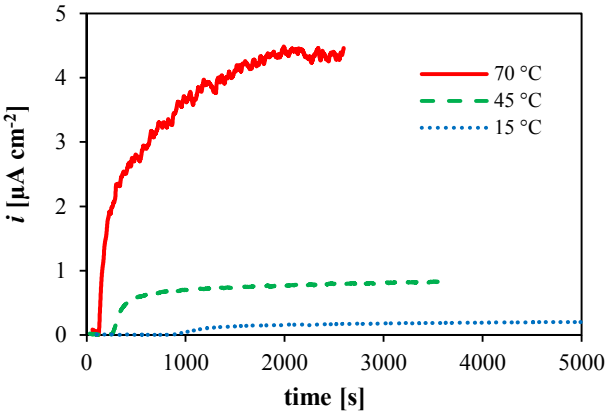

Fig. 9 – Second permeation transients for 3 wt% Ni sample when charging in 0.1 M NaOH at 15, 45 and 70 °C.

Fig. 13 shows C_0 as a function of Ni content and temperature. C_0 increased with increasing temperature for all Ni contents. At each temperature, C_0 decreased with increasing Ni content in the same manner as J_{ss} L.

Three consecutive permeation transients for each material were performed at 15 °C to evaluate irreversible trapping. Fig. 14 shows the permeation transients for the 3 wt% Ni sample at 15 °C plotted as steady-state normalized permeation flux (J) vs. the logarithm of normalized time. The time is normalized to the sample thickness (L) and to the Fe bcc lattice diffusion coefficient (D_l), Equation (2). Ideal Fe bcc lattice diffusion, calculated from the solution of Fick's second law given in ISO 17081 [37], is plotted for comparison. There was a short time shift between the first and the second, and between the second and third transients. The time shift was seen for all the materials except in the 0 wt% Ni case where all the transients overlapped. However, the time shifts were smaller than

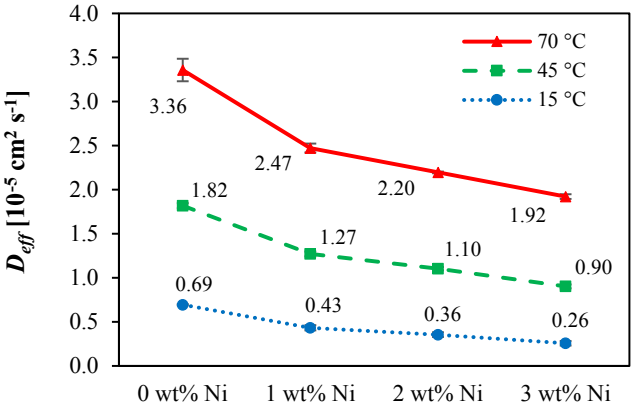

Fig. 10 – D_{eff} calculated by the t_b method for samples when charging in 0.1 M NaOH at 15, 45 and 70 °C. The markers represent the average of three consecutive permeation transients. Error bars show the standard deviations, which are smaller than the markers in most cases. Lines added to aid visualization.

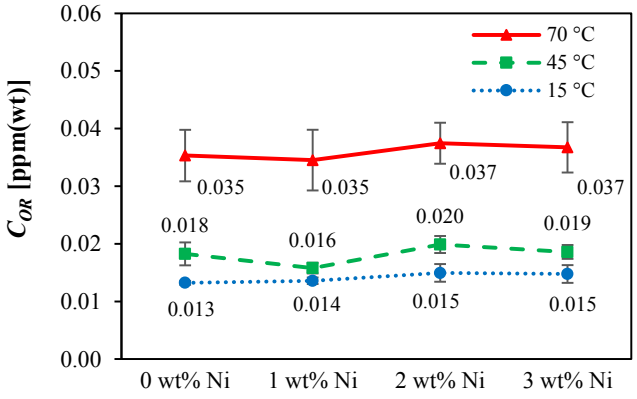

Fig. 11 – C_{OR} for samples when charging in 0.1 M NaOH at 15, 45 and 70 °C. The markers represent the average of three consecutive permeation transients. Error bars show the standard deviations. Lines added to aid visualization.

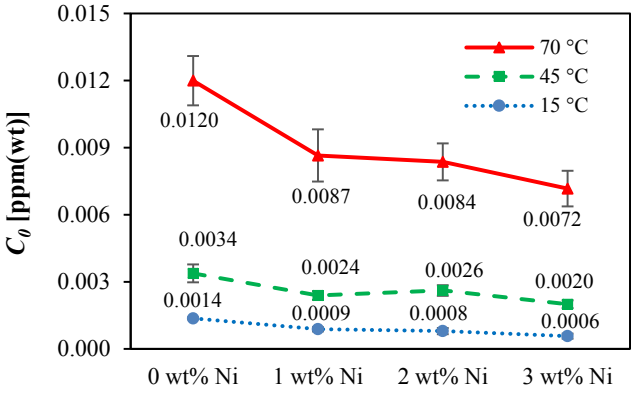

Fig. 13 – C_0 for samples when charging in 0.1 M NaOH at 15, 45 and 70 °C. The markers represent the average of three consecutive permeation transients. Error bars show the standard deviations, which are smaller than the markers in some cases. Lines added to aid visualization.

what would be expected if resulting from irreversible trapping as discussed in section Effect of Ni on hydrogen permeation.

Evaluating the dependence of D_{eff} (t_b) with temperature, as described in section Analysis of the results, allowed the number and strength of reversible traps in the materials to be estimated. The linear fit of D_{eff} with temperature according to Equation (7) was excellent, with coefficients of determination (r^2) [48] above 0.999 in all cases. Table 3 shows N_r and E_b values as a function of Ni content in the LAS. E_b values are expressed as negative values as commonly done [44]. $|E_b|$ increased, while N_r decreased with increasing Ni content.

Aerated 3.5 wt% NaCl in the cathodic compartment

Fig. 15 shows the permeation transients for 0 and 2 wt% Ni samples at 15 °C when charging in aerated 3.5 wt% NaCl. t_b was shorter for 0 wt% Ni than for 2 wt% Ni. i_{ss} was about 3 times larger for the 0 wt% Ni sample than for the 2 wt% Ni sample. As seen in Fig. 15, the two permeation transients for 0 wt% Ni were identical. The two permeation transients for 2 wt% Ni stabilized at slightly different i_{ss}, but when plotted as steady-state normalized permeation flux vs. the logarithm of normalized time they were identical, without any time shift between the transients.

When hydrogen charging was done in aerated 3.5 wt% NaCl, the transients had well-defined i_{ss} values, allowing the use of the t_{lag} method to determine D_{eff}. Table 4 shows D_{eff} values calculated from both t_{lag} and t_b methods, together with J_{ss} L, C_0 and C_{OR} values. For both calculation approaches, D_{eff}

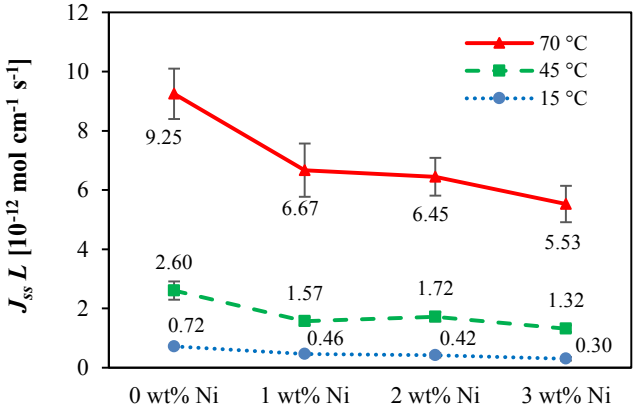

Fig. 12 – J_{ss} L for samples when charging in 0.1 M NaOH at 15, 45 and 70 °C. The markers represent the average of three consecutive permeation transients. Error bars show the standard deviations, which are smaller than the markers in some cases. Lines added to aid visualization.

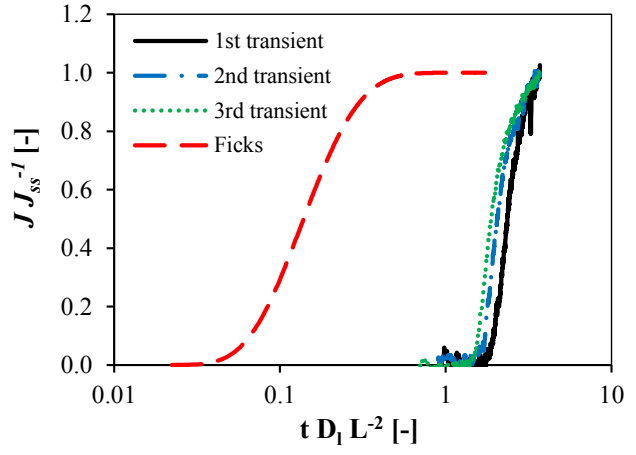

Fig. 14 – Permeation transients for 3 wt% Ni sample at 15 °C plotted as steady-state normalized permeation flux vs. the logarithm of normalized time. Ideal Fe bcc lattice diffusion ("Ficks") is plotted for comparison.

Table 3 – Estimated values of E_b and N_r of the LAS.

Alloy	E_b [kJ mol^{-1}]	N_r [sites cm^{-3}]
0 wt% Ni	−22.5	3.84 10^{20}
1 wt% Ni	−23.7	3.78 10^{20}
2 wt% Ni	−24.6	3.27 10^{20}
3 wt% Ni	−27.1	1.58 10^{20}

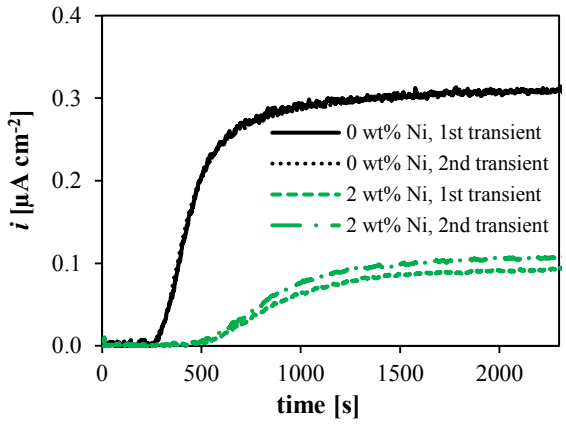

Fig. 15 – Permeation transients for 0 and 2 wt% Ni samples when charging in aerated 3.5 wt% NaCl at 15 °C. The curves for the 1st and 2nd transients on the 0 wt% Ni sample overlap and cannot be distinguished. Sample thickness for 0 and 2 wt% Ni samples differed only by 0.02 mm [< 2% of total sample thickness], hence normalized axes are not used. Time zero is when a cathodic current was supplied from the potentiostat.

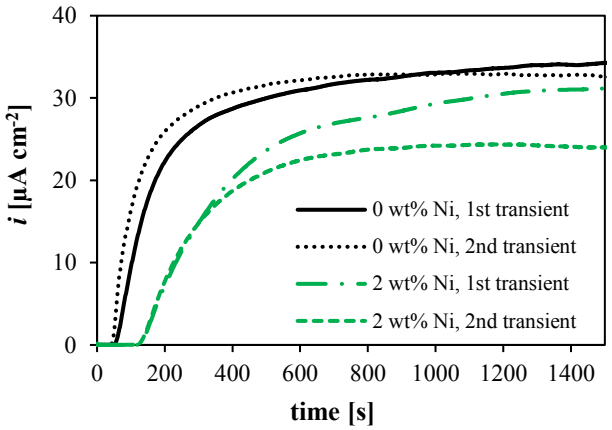

Fig. 16 – Permeation transients for 0 and 2 wt% Ni samples when charging in the electrolyte containing a hydrogen recombination poison at 15 °C. Note the 100X increase in i-scale compared to Fig. 15. Sample thickness for 0 and 2 wt% Ni samples differed only by 0.02 mm [< 2% of total sample thickness], hence normalized axes are not used. Time zero is when a cathodic current was supplied from the potentiostat.

was about twice as large for the 0 wt% Ni material as for the 2 wt% Ni sample. C_{OR}, whether calculated with D_{eff} from t_{lag} or t_b methods, was about 1.6 times larger for the 0 wt% Ni sample than for the 2 wt% Ni sample.

Hydrogen recombination poison in the cathodic compartment

Fig. 16 shows the permeation transients performed at 15 °C when charging in the electrolyte containing a hydrogen recombination poison. t_b was shorter for 0 wt% Ni than for 2 wt% Ni. i_{ss} was higher for the 0 wt% Ni sample than for the 2 wt% Ni sample, but the transients on the 2 wt% Ni sample showed a large variation of 6.8 µA cm^{-2}. Dark surface films formed on the hydrogen charging sides of the samples whose extent varied from test to test. Slightly changing surface conditions yielded the consecutive permeation transients slightly different, but there was no significant time shift between them.

When charging in the electrolyte containing a hydrogen recombination poison, the transients obtained well-defined i_{ss} values within a reasonable time and D_{eff} was calculated by both the t_{lag} and the t_b method. Table 5 shows D_{eff} values calculated by both methods, together with J_{ss} L, C_0 and C_{OR} values. For both calculation methods, D_{eff} was more than twice as large for the 0 wt% Ni sample than for the 2 wt% Ni sample. Likewise, C_{OR}, whether calculated with D_{eff} from t_{lag} or t_b methods, was about twice as large for the 2 wt% Ni sample than for the 0 wt% Ni sample.

Discussion

Materials characterization

As explained by Samuels [49], banding can be described as "the preferential grouping of ferrite and pearlite in alternate bands aligned in the rolling direction", and is a consequence of an inhomogeneous distribution of alloying elements. The received plate materials had severe banding as seen in Fig. 3, which was successfully removed by the homogenization heat treatment. It was considered important to remove the banding since it may have a direct effect on hydrogen diffusion [50] and steels containing Ni are prone to banding [49].

Effects of Ni on phase equilibria

The refining effects of Ni on the microstructure of LAS, as seen in Fig. 4, are well known [13]. Ni does not form secondary phases and remains in solid solution in the ferrite phase up to about 7 wt% [1,13]. Because Ni is an austenite stabilizing

Table 4 – Data resulting from hydrogen permeation transients on 0 and 2 wt% Ni samples when charging in aerated 3.5 wt% NaCl at 15 °C.

	D_{eff} (t_{lag}) [cm^2 s^{-1}]	D_{eff} (t_b) [cm^2 s^{-1}]	i_{ss} [µA cm^{-2}]	C_{OR} (t_{lag}) [ppm (wt)]	C_{OR} (t_b) [ppm (wt)]	J_{ss} L [mol cm^{-1} s^{-1}]	C_0 [ppm (wt)]
0 wt% Ni, 1st transient	$4.50\ 10^{-6}$	$2.74\ 10^{-6}$	$2.99\ 10^{-1}$	$9.94\ 10^{-3}$	$1.63\ 10^{-2}$	$3.50\ 10^{-13}$	$6.65\ 10^{-4}$
0 wt% Ni, 2nd transient	$4.45\ 10^{-6}$	$2.80\ 10^{-6}$	$3.01\ 10^{-1}$	$1.01\ 10^{-2}$	$1.60\ 10^{-2}$	$3.51\ 10^{-13}$	$6.66\ 10^{-4}$
2 wt% Ni, 1st transient	$2.20\ 10^{-6}$	$1.49\ 10^{-6}$	$9.29\ 10^{-2}$	$6.23\ 10^{-3}$	$9.23\ 10^{-3}$	$1.07\ 10^{-13}$	$2.04\ 10^{-4}$
2 wt% Ni, 2nd transient	$2.28\ 10^{-6}$	$1.55\ 10^{-6}$	$1.06\ 10^{-1}$	$6.81\ 10^{-3}$	$1.01\ 10^{-2}$	$1.22\ 10^{-13}$	$2.31\ 10^{-4}$

Table 5 – Data resulting from hydrogen permeation transients on 0 and 2 wt% Ni samples when charging in the electrolyte containing a hydrogen recombination poison at 15 °C.

	D_{eff} (t_{lag}) [$cm^2\ s^{-1}$]	D_{eff} (t_b) [$cm^2\ s^{-1}$]	i_{ss} [$\mu A\ cm^{-2}$]	C_{OR} (t_{lag}) [ppm (wt)]	C_{OR} (t_b) [ppm (wt)]	$J_{ss}\ L$ [$mol\ cm^{-1}\ s^{-1}$]	C_0 [ppm (wt)]
0 wt% Ni, 1st transient	$1.03\ 10^{-5}$	$1.41\ 10^{-5}$	35.23	0.50	0.37	$4.05\ 10^{-11}$	$7.69\ 10^{-2}$
0 wt% Ni, 2nd transient	$1.56\ 10^{-5}$	$1.73\ 10^{-5}$	32.80	0.31	0.28	$3.75\ 10^{-11}$	$7.11\ 10^{-2}$
2 wt% Ni, 1st transient	$5.14\ 10^{-6}$	$6.08\ 10^{-6}$	31.84	0.91	0.77	$3.66\ 10^{-11}$	$6.94\ 10^{-2}$
2 wt% Ni, 2nd transient	$6.51\ 10^{-6}$	$6.11\ 10^{-6}$	24.30	0.54	0.58	$2.78\ 10^{-11}$	$5.27\ 10^{-2}$

element, it expands the austenite region in the phase diagram and lowers the eutectoid temperature [51]. As a result, the LAS grain sizes are refined with increasing Ni content [13], as it can be seen when comparing the materials cooled at the same rate, i.e., 0 and 1 wt% Ni and 2 and 3 wt% Ni. A consequence of the lowered transformation temperature is that Ni also promotes the formation of acicular ferrite [13,52], which has been observed for Ni contents above 1 wt% in ferritic/pearlitic steels by others [13,52].

The interlamellar pearlite spacing is determined solely by the transformation temperature, with finer pearlite lamella forming at lower transformation temperatures [53]. The finer pearlite lamellar spacing in 1 wt% Ni compared to 0 wt% Ni, and in 3 wt% Ni compared to 2 wt% Ni can then be explained by the lowering of the eutectoid temperature with increasing Ni content. The decrease in eutectoid temperature causes the transformation to begin at lower temperatures for higher Ni contents when cooled at the same rate. The fact that the 2 wt% Ni samples had larger interlamellar spacing than 1 wt% Ni can be explained by the slower cooling rate, causing the transformation to progress at a higher temperature.

With the addition of Ni, the eutectoid composition is shifted towards a lower carbon content [51], and from the "lever rule", it can be inferred that the fraction of pearlite increased at the expense of ferrite. The influence of Ni on the eutectoid composition explains the increase in the pearlite fraction from about 0.2 to about 0.3 when the Ni content increased from 0 to 3 wt%, Fig. 5, which is an unavoidable complication when keeping the chemical composition, outside the Ni content, fixed.

Experimental challenges and considerations

When charging in 0.1 M NaOH, *i* did not stabilize at clear steady-state values, but rose monotonically, as seen in Figs. 8 and 9. Challenges with unsteady surface conditions on the hydrogen charging side have been reported previously by Zakroczymski [54], who investigated the permeation of iron by cathodically generating hydrogen in a 0.1 M NaOH solution. In this case, a barrier layer formed on the sample surface at OCP, which hampered the entry of hydrogen after switching to cathodic charging. During cathodic charging, the surface barrier was gradually removed by a reduction process [54], although Zakroczymski et al. [55] showed later on that it was probably never completely removed. Zakroczymski et al. [55] found, using ellipsometry, that the surface layer changed with time during cathodic charging. As a result, the permeation current on the anodic side continued to increase for up to 50 h before a constant flux was obtained. Casanova and Crousier [56] suggested that such changes could be related either to a low diffusion coefficient of the gradually diminishing surface layer or to a gradually changing surface coverage of adsorbed hydrogen with time.

The choice of i_{ss} when charging in 0.1 M NaOH affected the calculated values of D_{eff} (using the t_{lag} method) and C_{OR} directly. As an example, if i_{ss} was chosen at the end of the permeation transients for the 3 wt% Ni sample, Fig. 9, both at 45 and 70 °C, the resulting D_{eff} values, calculated from the t_{lag} method, were almost equal. When using the t_b method, D_{eff} was higher at 70 °C than at 45 °C as would have been expected. The large increase in *i* seen from about 300 to 2500 s at 70 °C may be due to a significant alteration of a surface barrier on the cathodic sample side at this temperature. Thus, only the t_b method was used to calculate D_{eff} from transients obtained when charging in 0.1 M NaOH to circumvent this challenge. With the same reasoning, Luppo and Ovejero-Garcia [34] chose the t_b method when performing hydrogen permeation tests on LAS with hydrogen charging in 0.1 M NaOH. The preferred use of the t_b method over the t_{lag} method when there are layers impeding hydrogen diffusion has been discussed by Boes and Züchner [57]. In this work, only values based on the t_b method are discussed throughout this section to facilitate the comparison between experiments performed with different electrolytes in the cathodic compartment.

Herein, single values of D_{eff} were used to define the entire permeation transients. This approach is only valid for low trap occupancy, i.e., the fraction of reversible traps occupied <<1 [35,45]. Qualitatively, if trap occupancy is high, the diffusion coefficient will continually change during the permeation transient, appearing faster as traps fill up [35]. In such a situation, the estimated single D_{eff} values will depend on the part of the curve used for the fit [44]. In the same way, calculating C_{OR} from Equation (3) becomes increasingly inaccurate as trap occupancy increases [58]. Trap occupancy increases with increasing trap strength, $|E_b|$, and increasing hydrogen concentration in the lattice, C_0 [35,45,59]. The trap occupancy can be approximated by dividing the value of C_{OR} (units recalculated from ppm (wt) to atoms cm^{-3}) by the number of reversible traps, *Nr* [45]. The C_{OR} value of 0.013 ppm (wt) for the 0 wt% Ni sample charged in 0.1 M NaOH at 15 °C herein, Fig. 11, corresponded to about $6.14\ 10^{16}$ H atoms cm^{-3}, and when divided by the estimated N_r, Table 3, the trap occupancy fraction was approximated to $1.60\ 10^{-4}$. When charging in the electrolyte containing a hydrogen recombination poison, the trap occupancy increased due to the increase in C_0, but the approximated trap occupancy fraction was still very low, < 0.005 for the 0 wt% Ni sample. Regardless of possible inaccuracies, it is acknowledged that it can be pragmatically useful to

calculate D_{eff} by simple analysis [35], e.g., to compare material variables under the same environmental severity on a qualitative basis [9].

Effect of Ni on hydrogen permeation

When charging in aerated 3.5 wt% NaCl, C_0 values were in the order of 0.001 ppm (wt), Table 4, which, according to Griffiths and Turnbull [58], is typical for cathodic protection of steels in neutral environments. Charging in 0.1 M NaOH at 15 °C gave C_0 values of the same magnitude, Fig. 13. When charging in the electrolyte containing thiosulfate as a hydrogen recombination poison, C_0 values were close to 0.1 ppm (wt), i.e., a 100 fold increase, which is characterized as severe charging [58]. Kappes et al. [59] performed hydrogen permeation experiments on American Petroleum Institute (API) X65 pipe steel exposed at OCP in 5 wt% NaCl + 0.5 wt% acetic acid with H_2S gas partial pressures ranging from 0.029 to 101.3 kPa. Testing was carried out at room temperature. The authors presented J_{ss} L values, which, from Equation (1), corresponds to C_0 values in the range 0.01–0.1 ppm (wt). In other words, the results obtained by polarizing in the electrolyte containing a hydrogen recombination poison should give a fair representation of the materials performance in an H_2S environment.

Fig. 10 shows that D_{eff} decreased with increasing Ni content at all tested temperatures when charging in 0.1 M NaOH. D_{eff} was 2.7 times larger for 0 wt% Ni than for 3 wt% Ni at 15 °C, 2.0 times larger at 45 °C and 1.8 times larger at 70 °C. D_{eff} for 0 wt% Ni at 45 °C was 2.6 times larger than D_{eff} for 0 wt% Ni at 15 °C; hence the effect of increasing the Ni content from 0 to 3 wt% was comparable to the effect of a 30 °C increase in temperature. Upon increasing temperature, traps with increasing energy cease to trap hydrogen [33]. The fact that the relative difference in D_{eff} between 0 and 3 wt% Ni decreased with increasing temperature could on a qualitative basis mean that some reversible trap sites, whose number increased with increasing Ni content, were emptied when the temperature increased. It may also, however, be related to a larger relative impact of the surface effects discussed in section Experimental challenges and considerations, at higher temperatures, which possibly affects all materials equally. A quantitative evaluation of reversible trap number and strength is discussed in section Trap characterization and direct and indirect effects of Ni alloying.

Charging in aerated 3.5 wt% NaCl and in an electrolyte containing a hydrogen recombination poison at 15 °C with 0 and 2 wt% Ni samples, confirmed that the diffusivity decreased with increasing Ni content. In aerated 3.5 wt% NaCl, D_{eff} (t_b) for the 0 wt% Ni sample was 1.8 times larger than for the 2 wt% Ni sample. With the electrolyte containing a hydrogen recombination poison, the same factor was 2.6, while in the 0.1 M NaOH electrolyte, the factor was 2.0.

The D_{eff} (t_b) values were largest when charging in the electrolyte containing a hydrogen recombination poison. The values were 5.7 times larger for the 0 wt% Ni material and 4.0 times larger for the 2 wt% Ni material compared to those obtained when charging in aerated 3.5 wt% NaCl. The increase in D_{eff} observed when charging in the electrolyte containing a hydrogen recombination poison could be explained by the known dependence of D_{eff} with hydrogen concentration [58]. C_0 was approximately two orders of magnitude larger when testing in the electrolyte containing a hydrogen recombination poison compared to the aerated 3.5 wt% NaCl solution. The examples presented by Griffiths and Turnbull [58] showed that this can result in more than one order of magnitude increase in D_{eff}. Trap occupancy increases with increasing hydrogen content in the lattice [35,45,59] and D_{eff} then approaches the D_l value [59]. These facts deemed it relevant to investigate the effect of Ni under severe hydrogen charging conditions as done with the electrolyte containing thiosulfate as hydrogen recombination poison. Increasing the hydrogen concentration shifted D_{eff} towards D_l, but did not reduce the relative difference between the 0 and 2 wt% Ni materials.

The values of D_{eff} (t_b) obtained for both 0 and 2 wt% Ni samples when charging in 0.1 M NaOH at 15 °C, were about 2.5 times larger than those obtained when charging in aerated 3.5 wt% NaCl electrolyte, even though the C_0 values were of similar magnitudes. Although D_{eff} values are inherently thickness independent [37], the observed difference may be a result of the thicker samples tested in the 0.1 M NaOH electrolyte (1.9 mm vs. 1.1 mm) with diminished relative delaying effects from surface processes for thicker samples [42], as discussed in section Experimental challenges and considerations. Since the permeation transients cannot outrun diffusion, it is commonly reasoned that the highest value of D_{eff} is the most representative [33] at a similar charging severity.

The correlation between C_{OR} and Ni content varied with the hydrogen charging conditions. When charging in 0.1 M NaOH the C_{OR} values - determined from Equation (3) using D_{eff} from the t_b method - showed no clear trend with Ni content at either of the tested temperatures. When charging in aerated 3.5 wt% NaCl, C_{OR} was highest for the 0 wt% Ni sample, while C_{OR} was highest for the 2 wt% Ni sample when charging with the electrolyte containing a hydrogen recombination poison.

The variation of C_{OR} with Ni content depends on the relative trends of J_{ss} L and D_{eff} with Ni content according to Equation (3). J_{ss} L decreased with increasing Ni content in all charging environments, but the average ratio of the J_{ss} L values between 0 and 2 wt% Ni samples at 15 °C, varied from 1.7 when charging in 0.1 M NaOH, to 3.1 when charging in aerated 3.5 wt % NaCl and 1.2 when charging in the electrolyte containing a hydrogen recombination poison. At the same conditions, the average ratios of the D_{eff} (t_b) values between the 0 and 2 wt% Ni samples ranged from 1.8 to 2.6, thus showing less variation with the charging environment than the J_{ss} L ratios.

D_l is generally considered to be independent of steel microstructure and composition as long as the steel has a bcc structure [43,44,60]. As such, the decrease in J_{ss} L with increasing Ni content seen in all charging conditions, is considered to result from a decrease in C_0 with increasing Ni content according to Equation (1) [1]. C_0 increases with increasing surface coverage of adsorbed hydrogen, H_{ads} [61]. The surface coverage of H_{ads} is determined by details of the mechanism for the hydrogen evolution reaction and the kinetic properties of the sample surface in the different electrolytes [61]. Ni generally enhances the kinetics of the hydrogen evolution reaction relative to Fe [38] by promoting the hydrogen desorption reaction [14]. However, a detailed evaluation of the effect of Ni on the surface coverage of H_{ads}

under the different charging conditions is complicated and outside the scope of this work. Since different mechanisms may control hydrogen entry to the LAS in the different charging conditions, it is not surprising that the relative impact of Ni on C_0 varies between the three charging conditions. In particular, when charging in the electrolyte containing the thiosulfate recombination poison, hydrogen entry involves the formation of H_2S and iron sulfide films [39,40], which processes may show a different dependence on Ni content in the LAS than cathodic hydrogen evolution in 0.1 M NaOH or aerated 3.5 wt% NaCl.

Since D_{eff} decreased with increasing Ni content in all charging conditions, Equation (3) suggests that C_{OR} would have increased with increasing Ni content if all LAS were charged to the same value of $C_0/J_{ss}\,L$ in each environment. The effect of Ni on hydrogen uptake in service environments, e.g., at OCP in acidic brine containing H_2S, is another important aspect concerning the effect of Ni on SSC resistance [14,15]. A recent literature review [1] pointed out that in various environments, including acidic brine containing H_2S, adding Ni to QT LAS decreased the value of C_0. Similar results were obtained herein for ferritic/pearlitic LAS in three different charging conditions.

Irreversible trapping was evaluated by performing consecutive charge/discharge transients. There was a short time shift between the consecutive transients when testing in 0.1 M NaOH at 15 °C for all the materials except 0 wt% Ni, where all the transients were equally fast. The time shifts were exemplified by the 3 wt% Ni sample in Fig. 14. Time delays from the first to the second transients suggest irreversible trapping [37], but time delays from the second to the third transients would not be expected. Together with the fact that irreversible trapping is expected to delay the permeation transients in the range of 2–3 orders of magnitude [62], variations in surface conditions on the charging surface between the transients as discussed in section Experimental challenges and considerations are a more likely explanation. Manolatos et al. [63] have previously discussed how variations in the surface conditions may lead to erroneous conclusions concerning trapping. Testing in aerated 3.5 wt% NaCl and electrolytes containing a hydrogen recombination poison confirmed the absence of irreversible trapping. In these cases, the input surface conditions were identical for the first and the second transients and no time shifts were seen.

According to Turnbull et al. [9], it is unlikely that irreversible traps can be neglected in steels, as they observed a clear time delay in the first compared to the subsequent permeation transients when testing a martensitic stainless steel. Nevertheless, others have not observed this time shift. Bolzoni et al. [62] investigated two pipeline steel materials (API 5L X65 and ASME SA-182 F22) in as-received, fully quenched and annealed conditions, and did not observe time shifts between the permeation transients for any of the materials. Chan [19] performed permeation tests on martensitic Fe-Mn alloys with various carbon contents (Mn content not specified). The difference between the first and second permeation transient was absent for a material with 0.23 wt% C, but became increasingly evident as the carbon content increased up to 0.93 wt%. Chan suggested that, when the carbon content increased, quenching produced more microcracks, microvoids, and retained austenite that acted as irreversible traps.

Trap characterization and direct and indirect effects of Ni alloying

Because all alloying elements, including Ni, affect the phase equilibria of LAS, there were some microstructural dissimilarities between the materials, as discussed in section Materials characterization. Grain size and interlamellar pearlite spacing were not direct functions of Ni content, but the fraction of pearlite increased monotonically with increasing Ni content. The amount, location, and morphology of cementite affect hydrogen uptake and diffusion in steels [50,64–66]. Luppo and Ovejero-Garcia [34] revealed a preferential accumulation of hydrogen at cementite and ferrite-cementite interfaces over ferrite itself using a hydrogen microprint technique. Chan and Charles [64] investigated ferritic/pearlitic steels and found that the hydrogen content increased and the apparent (effective) diffusion coefficient decreased with increasing pearlite content, obtained by increasing the carbon concentration.

The quantitative trap characterization of the LAS provided E_b and N_r values as seen in Table 3. $|E_b|$ values from 15 to 18 kJ mol^{-1} associated with the ferrite/pearlite interface have been reported in the literature [65,67]. In this regard, the $|E_b|$ value of 22.5 kJ mol^{-1} for the 0 wt% Ni sample herein is not unlikely. $|E_b|$ values for Ni in solid solution (in pure Fe) have been estimated by Pressouyre [68] and Kedzierzawski [69] after the results of Beck et al. [16] and Dresler and Frohberg [17], respectively. $|E_b|$ was about 8 kJ mol^{-1} in the work of Beck et al. and roughly 18.4 kJ mol^{-1} in the work of Dresler and Frohberg. Herein, $|E_b|$ increased with increasing Ni content in the LAS. Considering the fact that $|E_b|$ values of Ni in solid solution (in pure Fe) presented in literature are similar to, or smaller than the $|E_b|$ values associated with pearlite, the average trap energy was not expected to increase with increasing Ni content in the LAS.

The N_r values herein were one order of magnitude lower than those found by Castaño Rivera et al. [32] in a cold-rolled API 5L X60 steel with a QT microstructure, while Robertson and Thompson [67] reported a one order of magnitude lower value than herein of 2 10^{19} traps cm^{-3} in a pearlitic steel with 0.43 wt% C by a rough estimate. Castaño Rivera et al. [32] made rough approximations on the expected number of traps from dislocations, ferrite-cementite interfaces and grain boundary sites in the QT API 5L X60 steel, but obtained N_r values that were one and two orders of magnitude smaller than those of the LAS herein. Estimating the number of traps with basis in the interfacial area between ferrite and pearlite in the LAS herein would be rather arbitrary and beyond the scope of the current work, but the number of traps is expected to increase as the fraction of pearlite increased in the LAS. Similarly, the number of traps from Ni in solid solution must increase with increasing Ni content, and 1 wt% Ni in solid solution corresponds to about 8.5 10^{20} atoms cm^{-3}. Both the direct and indirect effects of Ni alloying are expected to increase the number of traps in the LAS, and it is difficult to explain, with the results presented herein alone, the decrease found in N_r with increasing Ni content.

As experienced by Castaño Rivera et al. [32], assigning E_b and N_r values to a particular microstructural feature in the LAS is difficult. Although the values of E_b and N_r are of the same magnitudes as found by others, the trend with Ni content is questionable. One assumption for the analysis of trap number and strength was the presence of a single type of trap. Considering the complex microstructure of the LAS, it would be challenging to resolve the trend of E_b and N_r with Ni content with this model. The deconvolution of the direct effects of Ni in solid solution from its indirect influence on altering the phase equilibria of LAS is difficult, both by qualitative and quantitative means and it is the topic of future work.

Implications of the results

de Santa Maria and Turnbull [7] found that the cracking resistance of an AISI 410 steel (measured by slow strain rate testing) decreased with increasing J_{ss} L values (measured by permeation studies) when charged in brine of varying pH and H_2S concentration. The decrease in J_{ss} L with increasing Ni content observed herein, and by others [1], is considered beneficial [1,14]. However, since the material is indeed different when the Ni content changes - the trend of C_{OR} with Ni content varied with the charging conditions - a decrease in J_{ss} L with increasing Ni content does not necessarily imply a decreasing cracking susceptibility with increasing Ni content.

Nanis and Namboodhiri [70] demonstrated the essential role of the diffusion rate when hydrogen was not initially available at a location sensitive to cracking. Considering that the results of this investigation showed that Ni alloying delayed the hydrogen transport in the LAS, it would be tempting to assume that Ni could improve HSC resistance. However, the relationship between experimentally obtained D_{eff} and C_{OR} values and the resistance of a material to HSC or SSC is not fully understood. As stated by Koh et al. [71], SSC results from the combined action of hydrogen and metallurgical defects that are sensitive to HE. The sensitivity of a microstructural characteristic, e.g., Ni in solid solution, to HSC/SSC is not revealed by permeation experiments alone. Mechanical HE testing of the same materials is the scope of a separate publication [72].

Conclusions

The effect of nickel in ferritic/pearlitic research-grade low alloy steels on hydrogen uptake, diffusion, and trapping was evaluated by the electrochemical permeation method. Based on the results presented above, the following conclusions were drawn:

- The effective diffusion coefficient, D_{eff}, decreased with increasing Ni content at all tested temperatures and charging conditions.
- The sub-surface lattice hydrogen concentration, C_0, decreased with increasing Ni content in all charging conditions, while the dependence of the sub-surface hydrogen concentration in lattice and reversible trap sites, C_{OR}, with Ni content varied with the charging conditions.
- Irreversible trapping, evaluated by consecutive permeation transients, was not observed for any of the materials under any of the charging conditions.
- The fraction of pearlite increased with increasing Ni content. Separating the effect of Ni in the bcc lattice from the effect of the increasing pearlite fraction with increasing Ni content is difficult, and is the topic for future work.

Acknowledgements

This work is part of an international cooperation agreement between Norwegian University of Science and Technology (NTNU), General Electric (GE), Tenaris, YPF-Technología, and the Universidad Nacional de San Martin/Comisión Nacional de Energía Atómica (UNSAM/CNEA). NTNU and GE sponsored this work. The authors especially acknowledge the support of Dr. Alexander Fjeldly and Mr. Atle H. Qvale (GE).

REFERENCES

[1] Kappes M, Iannuzzi M, Rebak RB, Carranza RM. Sulfide stress cracking of nickel-containing low-alloy steels. Corrosion Rev 2014;32:101–28.
[2] ISO 15156-2. Petroleum and natural gas industries - materials for use in H_2S-containing environments in oil and gas production - Part 2: cracking-resistant carbon and low-alloy steels, and the use of cast irons. Geneva, Switzerland: International Organization for Standardization; 2015.
[3] Craig B, Brownlee J, Bruno T. Sulfide stress cracking of nickel steels. Corrosion 1992;48:90–7.
[4] Iannuzzi M, Barnoush A, Johnsen R. Materials and corrosion trends in offshore and subsea oil and gas production. npj Mater Degrad 2017;1.
[5] ASTM G193-12d. Standard terminology and acronyms relating to corrosion. West Conshohocken: ASTM International; 2012.
[6] ISO 15156-1. Petroleum and natural gas industries-Materials for use in H2S-containing environments in oil and gas production - Part I: General principles for selection of cracking-resistant materials. Geneva, Switzerland: International Organization for Standardization; 2015.
[7] de Santa Maria MS, Turnbull A. The effect of H 2 S concentration and pH on the cracking resistance of AISI 410 stainless steel in 5% brine. Corros Sci 1989;29:69–88.
[8] Hadam U, Zakroczymski T. Absorption of hydrogen in tensile strained iron and high-carbon steel studied by electrochemical permeation and desorption techniques. Int J Hydrogen Energy 2009;34:2449–59.
[9] Turnbull A, Carroll MW, Ferriss DH. Analysis of hydrogen diffusion and trapping in a 13% chromium martensitic stainless steel. Acta Metall 1989;37:2039–46.
[10] Turnbull A, de Santa Maria MS, Thomas N. The effect of H 2 S concentration and pH on hydrogen permeation in AISI 410 stainless steel in 5% NaCl. Corros Sci 1989;29:89–104.
[11] Zhang T, Zhao W, Deng Q, Jiang W, Wang Y, Wang Y, et al. Effect of microstructure inhomogeneity on hydrogen embrittlement susceptibility of X80 welding HAZ under pressurized gaseous hydrogen. Int J Hydrogen Energy 2017;42:25102–13.
[12] Cramer SD, Covino BS, Jr. ASM handbook, volume 13A - corrosion: fundamentals, testing, and protection: ASM International; p. 367–374.

[13] Razzak MA. Heat treatment and effects of Cr and Ni in low alloy steel. Bull Mater Sci 2011;34:1439–45.
[14] Wilde B, Kim C, Turn Jr J. The influence of noble metal additions on the sulfide corrosion performance of AISI 4130 steel. Corrosion 1982;38:515–24.
[15] Yoshino Y, Minozaki Y. Sulfide stress cracking resistance of low-alloy nickel steels. Corrosion 1986;42:222–33.
[16] Beck W, Bockris J, Genshaw M, Subramanyan P. Diffusivity and solubility of hydrogen as a function of composition in Fe-Ni alloys. Metall Trans 1971;2:883–8.
[17] Dresler W, Frohberg M. Diffusion Coefficient of H in the system Fe-Ni at 25 and 58 C. J Iron Steel Inst 1973;211: 298–302.
[18] Yamanishi Y, Tanabe T, Imoto S. Hydrogen permeation and diffusion through pure Fe, pure Ni and Fe–Ni alloys. Trans Jpn Inst Metals 1983;24:49–58.
[19] Chan SLI. Hydrogen trapping ability of steels with different microstructures. J Chin Inst Eng 1999;22:43–53.
[20] Becker WT, Shipley RJ. ASM handbook, volume 11-failure analysis and prevention: ASM International; p. 691–693.
[21] Kohno M, Makioka M, Kinoshita S, Suzuki A. Mechanical properties of vacuum carbon-deoxidized thick-wall 21/4Cr-1Mo steel forging. In: Sangdahl G, Semchyshen M, editors. STP 755-EB - application of 2¼Cr-1 Mo steel for thick-wall pressure vessels. West Conshohocken, PA: ASTM International; 1982. p. 208–27.
[22] ASTM E1019-11. Standard test methods for determination of carbon, sulfur, nitrogen, and oxygen in steel, iron, nickel, and cobalt alloys by various combustion and fusion techniques. West Conshohocken: ASTM International; 2011.
[23] ASTM E1479-99. Standard practice for describing and specifying inductively-coupled plasma atomic emission spectrometers. West Conshohocken: ASTM International; 2011.
[24] Andrews K. Empirical formulae for the calculation of some transformation temperatures. J Iron Steel Inst 1965;203:721–7.
[25] ASTM E112-12. Standard test methods for determining average grain size. West Conshohocken: ASTM International; 2012.
[26] Underwood EE. Quantitative stereology. Reading. Mass: Addison-Wesley; 1970.
[27] Vander Voort GF, Roósz A. Measurement of the interlamellar spacing of pearlite. Metallography 1984;17:1–17.
[28] ASTM G148-97. Standard practice for evaluation of hydrogen uptake, permeation, and transport in metals by an electrochemical technique. West Conshohocken: ASTM International; 2011.
[29] Manolatos P, Jerome M, Galland J. Necessity of a palladium coating to ensure hydrogen oxidation during electrochemical permeation measurements on iron. Electrochim Acta 1995;40:867–71.
[30] Bruzzoni P. Efectos de superficie en la difusión de hidrógeno en hierro y aleaciones ferrosas. Universidad de Buenos Aires; 2003.
[31] Bruzzoni P, Carranza RM, Collet Lacoste JR. Influence of palladium films on hydrogen gas entry into iron: a study by electrochemical impedance spectroscopy. Int J Hydrogen Energy 2000;25:61–5.
[32] Castaño Rivera P, Ramunni VP, Bruzzoni P. Hydrogen trapping in an API 5L X60 steel. Corros Sci 2012;54:106–18.
[33] Hirth J. Effects of hydrogen on the properties of iron and steel. Metall Trans A 1980;11:861–90.
[34] Luppo M, Ovejero-Garcia J. The influence of microstructure on the trapping and diffusion of hydrogen in a low carbon steel. Corros Sci 1991;32:1125–36.
[35] Turnbull A. Perspectives on hydrogen uptake, diffusion and trapping. Int J Hydrogen Energy 2015;40:16961–70.
[36] Devanathan M, Stachurski Z. The adsorption and diffusion of electrolytic hydrogen in palladium. In: Proceedings of the Royal society of London a: mathematical, physical and engineering sciences. The Royal Society; 1962. p. 90–102.
[37] ISO 17081:2014. Method of measurement of hydrogen permeation and determination of hydrogen uptake and transport in metals by an electrochemical technique. Geneva, Switzerland: International Organization for Standardization; 2014.
[38] Hamann C, Hamnett A, Vielstich W. Electrochemistry, 2nd completely revised and updated. Weinheim: Wiley-VCH Pub; 2007. p. 98–102. 212-3.
[39] Kappes M, Frankel GS, Sridhar N, Carranza RM. Reaction paths of thiosulfate during corrosion of carbon steel in acidified brines. J Electrochem Soc 2012;159:C195–204.
[40] Tsujikawa S, Miyasaka A, Ueda M, Ando S, Shibata T, Haruna T, et al. Alternative for evaluating sour gas resistance of low-alloy steels and corrosion-resistant alloys. Corrosion 1993;49:409–19.
[41] Abd Elhamid M, Ateya G, Weil K, Pickering H. Effect of thiosulfate and sulfite on the permeation rate of hydrogen through iron. Corrosion 2001;57:428–32.
[42] Wach S, Miodownik AP, Mackowiak J. The diffusion of hydrogen through pure iron membranes. Corros Sci 1966;6: 271–85.
[43] Turnbull A, Carroll MW. The effect of temperature and H2S concentration on hydrogen diffusion and trapping in a 13% chromium martensitic stainless steel in acidified NaCl. Corros Sci 1990;30:667–79.
[44] Turnbull A. 4-Hydrogen diffusion and trapping in metals A2-Gangloff, Richard P. In: Somerday BP, editor. Gaseous hydrogen embrittlement of materials in energy technologies. Woodhead Publishing; 2012. p. 89–128.
[45] Oriani RA. The diffusion and trapping of hydrogen in steel. Acta Metall 1970;18:147–57.
[46] Turnbull A, Hinds G. Hydrogen diffusion in corrosion resistant alloys. Corrosion. New Orleans, LA, USA: NACE International; 2004.
[47] Aylward GH, Findlay TJV. SI chemical data. 5th ed. Milton: Wiley; 2002.
[48] Patience GS. Experimental methods and instrumentation for chemical engineers. Elsevier; 2013.
[49] Samuels LE. Light microscopy of carbon steels: ASM International; p. 110–8.
[50] Lee H-L, Lap-Ip Chan S. Hydrogen embrittlement of AISI 4130 steel with an alternate ferrite/pearlite banded structure. Mater Sci Eng 1991;142:193–201.
[51] Krauss G. Steels - processing, structure, and performance (2nd Edition). ASM International; p. 17–38.
[52] Koval V, Karvatskii L, Koval'chuk R. Influence of carbon, nickel, manganese, and vanadium on stress-corrosion cracking of steels in a medium containing hydrogen sulfide. Sov Mater Sci: a transl of Fiziko-khimicheskaya mekhanika materialov/Acad Sci Ukrainian SSR 1979;15:161–4.
[53] Davis JR. Metals handbook, desk edition (2nd Edition). ASM International; p. 152–173.
[54] Zakroczymski T. Permeability of iron to hydrogen cathodically generated in 0.1 M NaoH. Scripta Metall 1985;19:521–4.
[55] Zakroczymski T, Szklarska-Smialowska Z, Zakroczymski T. Activation of the iron surface to hydrogen absorption resulting from a long cathodic treatment in NaOH solution. J Electrochem Soc 1985;132:2548–52.
[56] Casanova T, Crousier J. The influence of an oxide layer on hydrogen permeation through steel. Corros Sci 1996;38: 1535–44.

[57] Boes N, Züchner H. Electrochemical methods for studying diffusion, permeation and solubility of hydrogen in metals. J Less Common Met 1976;49:223–40.
[58] Griffiths AJ, Turnbull A. On the effective diffusivity of hydrogen in low alloy steels. Corros Sci 1995;37:1879–81.
[59] Kappes M, Frankel GS, Thodla R, Mueller M, Sridhar N, Carranza RM. Hydrogen permeation and corrosion fatigue crack growth rates of X65 pipeline steel exposed to acid brines containing thiosulfate or hydrogen sulfide. Corrosion 2012;68:1015–28.
[60] Johnson D, Wu J. Hydrogen transport in carbon steels as a function of carbon content and heat treatment near 298 K. J Mater Energy Syst 1987;8:402–8.
[61] Cottis RA. 2.10-Hydrogen embrittlement. In: Stott Bcgllrs, editor. Shreir's corrosion. Oxford: Elsevier; 2010. p. 902–22.
[62] Bolzoni F, Re G, Ormellese M, Fallahmohammadi E, Fumagalli G, Lazzari L. Electrochemical investigation of hydrogen diffusion in pipeline steels. Corrosion. Orlando, FL, USA: NACE International; 2013.
[63] Manolatos P, Duret-Thual C, Le Coze J, Jerome M, Bollinger E. The electrochemical permeation of hydrogen in steels without palladium coating. Part II: study of the influence of microstructure on hydrogen diffusion. Corros Sci 1995;37:1785–96.
[64] Chan S, Charles J. Effect of carbon content on hydrogen occlusivity and embrittlement of ferrite–pearlite steels. Mater Sci Technol 1986;2:956–62.
[65] Jeng HW, Chiu LH, Johnson DL, Wu JK. Effect of pearlite morphology on hydrogen permeation, diffusion, and solubility in carbon steels. Metall Trans A 1990;21:3257–9.
[66] Luu WC, Wu JK. The influence of microstructure on hydrogen transport in carbon steels. Corros Sci 1996;38:239–45.
[67] Robertson WM, Thompson AW. Permeation measurements of hydrogen trapping in 1045 steel. Metall Trans A 1980;11:553–7.
[68] Pressouyre G. A classification of hydrogen traps in steel. Metall Mater Trans A 1979;10:1571–3.
[69] Kedzierzawski P. Hydrogen trapping in iron and iron alloys. Noyes publications, hydrogen degradation of ferrous alloys. 1985. p. 271–88.
[70] Nanis L, Namboodhiri TKG. Analysis of the permeation technique for the study of hydrogen entry into iron-base alloys. Stress corrosion cracking and hydrogen embrittlement of iron base alloys. Houston, TX, USA: NACE International; 1977.
[71] Koh SU, Kim JS, Yang BY, Kim KY. Effect of line pipe steel microstructure on susceptibility to sulfide stress cracking. Corrosion 2004;60:244–53.
[72] Husby H, Wagstaff P, Iannuzzi M, Johnsen R, Kappes M. Effect of nickel on the hydrogen stress cracking resistance of ferritic/pearlitic low alloy steels. 2018. To be published.